The South American rainfall dipole: A complex network analysis of extreme events

Niklas Boers[1,2], Aljoscha Rheinwalt[1,2], Bodo Bookhagen[3,4], Henrique M. J. Barbosa[5], Norbert Marwan[2], José Marengo[6], and Jürgen Kurths[1,2,7]

[1]Department of Physics, Humboldt University, Berlin, Germany, [2]Potsdam Institute for Climate Impact Research, Potsdam, Brandenburg, Germany, [3]Department of Geography, University of California, Santa Barbara, California, USA, [4]Now at Institute of Earth- and Environmental Sciences, University of Potsdam, Potsdam, Germany, [5]Department of Physics, University of Saõ Paulo, São Paulo, Brazil, [6]CCST INPE, Cachoeira Paulista, São Paulo, Brazil, [7]Department of Control Theory, Nizhny Novgorod State University, Nizhny Novgorod, Russia

Abstract Intraseasonal rainfall variability of the South American monsoon system is characterized by a pronounced dipole between southeastern South America and southeastern Brazil. Here we analyze the dynamical properties of extreme rainfall events associated with this dipole by combining a nonlinear synchronization measure with complex networks. We make the following main observations: (i) Our approach reveals the dominant synchronization pathways of extreme events for the two dipole phases, (ii) while extreme rainfall synchronization in the tropics is directly driven by the trade winds and their deflection by the Andes mountains, extreme rainfall propagation in the subtropics is mainly dictated by frontal systems, and (iii) the well-known rainfall dipole is, in fact, only the most prominent mode of an oscillatory pattern that extends over the entire continent. This provides further evidence that the influence of Rossby waves, which cause frontal systems over South America and impact large-scale circulation patterns, extends beyond the equator.

1. Introduction

We aim at an improved understanding of the characteristics and origins of extreme rainfall (above the 90th percentile of wet days) in the two most densely populated areas in South America, namely, southeastern South America (SESA) around Buenos Aires between 30°S and 35°S and southeastern Brazil (SEBRA) including Saõ Paulo and Rio de Janeiro between 18°S and 23°S (see Figure 1).

Large parts of the economies in these two regions depend on agriculture. They are thus heavily reliant on continuous water supply for irrigation and energy generation but also particularly vulnerable to damages caused by extreme rainfall and associated floodings and landslides [*Berbery and Barros*, 2002; *Carvalho et al.*, 2002; *Barros et al.*, 2006; *Marengo et al.*, 2013].

In large parts of South America, rainfall during the monsoon season (December to February, DJF) depends on atmospheric low-level moisture inflow from the tropical Atlantic Ocean to the Amazon Basin provided by the trade winds [*Zhou et al.*, 1998]. After crossing the Amazon Basin, the low-level winds are blocked by the Andes mountains and channeled southward, causing pronounced orographic rainfall peaks at the eastern slopes of the northern central Andes [e.g., *Bookhagen and Strecker*, 2008]. There exist two different regimes for the direction and strength of the subsequent low-level flow:

1. If the flow has a strong southward component, it establishes the South American Low-Level Jet (SALLJ) [*Marengo et al.*, 2004], transporting large amounts of moisture to northern Argentina and SESA. This regime is associated with enhanced rainfall [*Liebmann et al.*, 2004] and in particular with the formation of mesoscale convective systems [*Salio et al.*, 2007; *Durkee et al.*, 2009; *Boers et al.*, 2013] in SESA.
2. If the flow exhibits a pronounced eastward component, it transports moisture to the South Atlantic Convergence Zone (SACZ) and leads to enhanced rainfall in SEBRA [*Liebmann et al.*, 2004; *Carvalho et al.*, 2004].

The dipolar behavior of rainfall in SESA and SEBRA is the most important source of intraseasonal rainfall variability of the South American monsoon system [*Vera et al.*, 2006; *Marengo et al.*, 2004; *Jorgetti et al.*, 2013].
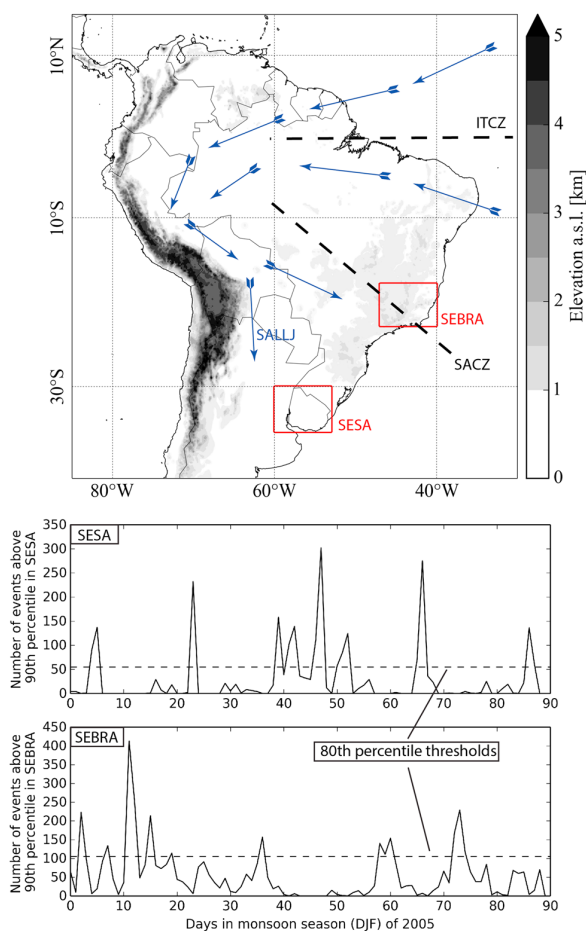
Figure 1. (top) Topography of South America and key features of the South American monsoon system (SAMS), including typical wind directions (blue arrows) and the South American Low-Level Jet (SALLJ). The climatological positions of the Intertropical Convergence Zone (ITCZ) and the South Atlantic Convergence Zone (SACZ) are shown by dashed black lines, while the two study areas, SESA (30°S to 35°S and 60°W to 53°W) and SEBRA (18°S to 23°S and 47°W to 40°W), are indicated by red boxes. (bottom) The time series of the number of extreme events in SESA (Figure 1, top) and SEBRA (Figure 1, bottom) for the monsoon season (DJF) of 2005. The 80th percentile thresholds that are used to define SESA and SEBRA phases are indicated by horizontal dashed lines.

Several studies have investigated the dipolar rainfall pattern between SESA and SEBRA during the monsoon season in South America. They mostly rely on principal component analysis (PCA) on the basis of daily mean values of precipitation or outgoing long-wave radiation (as a proxy for convection) data [*Nogués-Paegle and Mo*, 1997; *Liebmann et al.*, 2004; *Marengo et al.*, 2004; *Vera et al.*, 2006; *Marengo et al.*, 2012]. However, no corresponding characteristics of spatial covariability have been analyzed for extreme values so far, since PCA is not applicable for this purpose: PCA only includes the first two moments of the data distribution and is thus by construction not capable of capturing the characteristics of extreme events, which are located at the tail of the distribution. Furthermore, it is questionable, in general, to apply PCA to strongly non-Gaussian data distributions, since the resulting empirical orthogonal functions are, while uncorrelated, not independent and interpretation of their patterns is likely to be misleading [*Monahan et al.*, 2009].

Here we intend to fill this gap by employing a methodology which has recently been introduced to reveal and analyze the spatial characteristics of extreme rainfall covariability [*Malik et al.*, 2012; *Boers et al.*, 2013, 2014]. This method is based on the combination of a nonlinear synchronization measure and complex network theory.

2. Data

We employ satellite-derived rainfall data from the Tropical Rainfall Measurement Mission (TRMM 3B42 V7 [*Huffman et al.*, 2007]) with daily temporal and 0.25° × 0.25° spatial resolutions. Geopotential height and wind fields at 850 mbar are obtained from NASA's Modern-Era Retrospective Analysis for Research and Applications (MERRA) [*Rienecker et al.*, 2011] on daily temporal and 1/2° × 2/3° spatial resolutions. The spatial domain is confined to the coordinates 40°S to 15°N and 85°W to 30°W (Figure 1). All data sets are analyzed for the monsoon seasons (December to February, DJF) between 1998 and 2012.

3. Methods
3.1. Extreme Rainfall Events
We define extreme rainfall events as days on which rainfall amounts exceed the 90th percentile of the rainfall distribution restricted to days with rainfall sums larger than 0.01 mm/d. This percentile threshold is local in the sense that it depends on the respective grid cell's rainfall distribution.

3.2. Phases of the Rainfall Dipole

We define the two phases of the rainfall dipole between SESA and SEBRA on the basis of extreme rainfall event frequencies in the two regions. The SESA (SEBRA) phase of the dipole is defined as the set of days on which the sum of extreme events in the entire spatial domain of the SESA (SEBRA) box exceeds the 80th percentile (Figure 1). Note that these definitions are by construction independent in the sense that the SESA (SEBRA) phase only depends on the number of events in the SESA (SEBRA) box. Nevertheless, there is no temporal overlap between the two phases, which can be explained by the dipolar rainfall pattern between the two regions.

This amounts to an average of 18 active days for both SESA and SEBRA phases per DJF season. Composites of rainfall, geopotential height, and wind, as well as complex networks, will in the following be constructed separately for these two phases.

3.3. Event Synchronization

We consider an event-based measure of similarity to quantify the covariability of extreme rainfall at different grid cells. For this purpose, we employ event synchronization (ES), modified on the basis of *Quiroga et al.* [2002]. Consider two event series $\{e_i^\mu\}_{1\le\mu\le l_i}$ and $\{e_j^\nu\}_{1\le\nu\le l_j}$ with l_i respectively l_j events at grid points i respectively j, where e_i^μ denotes the time index of the μth event observed at grid point i. In order to decide if two events e_i^μ and e_j^ν can be uniquely assigned to each other, we first compute the waiting times between events $d_{ij}^{\mu,\nu} := |e_i^\mu - e_j^\nu|$. On this basis, we define the *dynamical delay*

$$\tau_{ij}^{\mu\nu} = \min \frac{\left\{ d_{ii}^{\mu,\mu-1}, d_{ii}^{\mu,\mu+1}, d_{jj}^{\nu,\nu-1}, d_{jj}^{\nu,\nu+1} \right\}}{2} \tag{1}$$

To exclude unreasonably long delays between events at different locations, we introduce a maximum delay $\tau_{\max}$. If $d_{ij}^{\mu,\nu} \le \tau_{ij}^{\mu\nu}$ and $d_{ij}^{\mu,\nu} < \tau_{\max}$, we count this as synchronous events:

$$S_{ij}^{\mu\nu} = \begin{cases} 1 & \text{if} \quad d_{ij}^{\mu,\nu} \le \tau_{ij}^{\mu\nu} \quad \text{and} \quad d_{ij}^{\mu,\nu} \le \tau_{\max}; \\ 0 & \text{else.} \end{cases} \tag{2}$$

ES between e_i and e_j is given as the sum of all $S_{ij}^{\mu\nu}$ (for fixed i and j)

$$\text{ES}_{ij} := \sum_{\mu\nu} S_{ij}^{\mu\nu}. \tag{3}$$

Each value ES_{ij} thus gives the number of events at grid points i and j which occurred synchronously (i.e., could be uniquely assigned to each other) within $\tau_{\max}$ days. This procedure is performed for all combinations of grid points i and j, with $1 \le i,j \le N = 48,400$. One advantage of this similarity measure is that it accounts for varying temporal delays between events at different grid cells within the prescribed maximum delay $\tau_{\max}$. In contrast, the classical lead-lag analysis on the basis of Pearson's correlation coefficient only yields one lead or lag for the entire time series.

3.4. Complex Networks: Construction

We will construct two separate networks for the two phases of the dipole in the following way: For the computation of the matrix $\{\text{ES}_{ij}\}_{1\le i,j\le N}$ for the SESA (SEBRA) phase, we will only consider those events in the time series $\{e_i^\mu\}_{1\le\mu\le l_i}$, which fall into the SESA (SEBRA) oscillation phase and ignore the remaining events.

For each grid cell (i,j), we need to estimate the statistical significance of the value ES_{ij}. For this purpose, we construct a null model assuming that the l_i events at i and l_j events at j are placed independently according to a uniform distribution: We construct 1000 surrogate pairs of an event time series for each combination of event numbers (l_i, l_j). By computing ES for all these pairs, we obtain a relative frequency distribution of values of ES consistent with the assumptions of the null model and infer the score of the 95% significance level from this distribution. Denoting this score by T, a network link will be placed between grid cells i and j if the corresponding value ES_{ij} is above T. For two arbitrary grid cells i and j, this can be formally written as

$$A_{ij} = \Theta(\text{ES}_{ij} - T(l_i, l_j)) - \delta_{ij}, \tag{4}$$

where Θ denotes the Heaviside function and Kronecker's delta δ is added to exclude links from a grid cell to itself.

3.5. Complex Networks: Application

In this study, we consider two network measures. First, we compute the degree (DG). At a given network node i, DG_i is defined as the number of other nodes to which this node is connected to by a network link:

$$DG_i := \sum_{j=1}^{N} A_{ij} \tag{5}$$

Thus, DG at a given grid cell yields the number of other grid cells where extreme events occur synchronously with extreme events at that grid cell. A region with high DG will therefore be interpreted as a region, which is particularly important for spatial distribution and thus propagation of extreme rainfall.

In addition, we are interested in the directions along which extreme events occur synchronously. For this purpose, we employ the measure directionality (DR). At each node (i.e., grid cell) i, this measure yields two values: the dominant angle DR_i^{ϕ} among all network links at that node and the strength DR_i^s corresponding to that angle, quantified as the number of links pointing in that direction. Let ϕ_{ij} denote the angle between the meridian going through node i and the straight line between node i and j. Since the networks considered in this study are undirected, all angles ϕ_{ij} are taken as *modulo* π, thus $\phi_{ij} \in [0, \pi)$. In the following, we will therefore refer to DR_i^{ϕ} as an *orientation* rather than an angle. We first compute the frequency distribution of all orientations φ of links at i:

$$P_i(\varphi) = \sum_{j \,:\, \phi_{ij} \in (\varphi - \epsilon, \varphi + \epsilon)} A_{ij} \,, \tag{6}$$

where we consider all orientations differing by less than $\epsilon = 0.02$ as equal. DR is then defined by the maximum of this distribution

$$DR_i^s = \max_{\varphi \in [0, \pi)} P_i(\varphi) \tag{7}$$

together with the corresponding orientation

$$DR_i^{\phi} = \arg \max_{\varphi \in [0, \pi)} P_i(\varphi) \,. \tag{8}$$

This measure can be visualized by streamlines which are, at each grid point, directed along the orientation given by DR. The DR strength DR_i^s will in the following be indicated by the thickness of these streamlines. In order to be able to obtain a clear interpretation, we will compute DR only for networks constructed for *simultaneous* events ($\tau_{max} = 0$). By construction, extreme rainfall at grid points which lie on the same streamline occur typically at the same day. In this sense, they can be interpreted as *isochrones*. Under the assumption that the temporal resolution of 1 day is sufficiently high, we thus expect that rainfall clusters typically propagate perpendicular to these streamlines.

4. Results

4.1. Atmospheric Conditions

Composites of geopotential height and wind fields constructed separately for the two different dipole phases show distinctively different features (Figure 2). As expected, we find anomalously high rainfall amounts over SESA for the SESA phase but negative anomalies over SEBRA (Figure 2, top row). We further observe relatively low-pressure values over SESA, which are associated with frontal systems initiated by Rossby wave-type patterns originating from the western Pacific Ocean [*Siqueira and Machado*, 2004; *Liebmann et al.*, 2004; *Seluchi and Garreaud*, 2006]. This low-pressure system extends northwestward along the eastern slopes of the southern Central Andes up to central Bolivia and forces the geostrophic low-level winds from the Amazon Basin southward along the eastern slopes of the Central Andes toward SESA [*Nicolini et al.*, 2002].

For SEBRA phases (Figure 2, bottom row), rainfall composites show pronounced positive rainfall anomalies over SEBRA but negative anomalies over SESA. There is a high-pressure system over northern Argentina and SESA and relatively low pressure over SEBRA. This pressure configuration inhibits the southward flow from the Amazon and instead turns it eastward toward the SACZ. There, we find clear indicators of an active convergence zone: northeasterly winds approaching from the tropical Atlantic as well as northwesterly winds originating from the western Amazon Basin all converge over the SACZ. These results are consistent with earlier studies on intraseasonal rainfall variability over South America [e.g., *Carvalho et al.*, 2002; *Liebmann et al.*, 2004; *Carvalho et al.*, 2004].
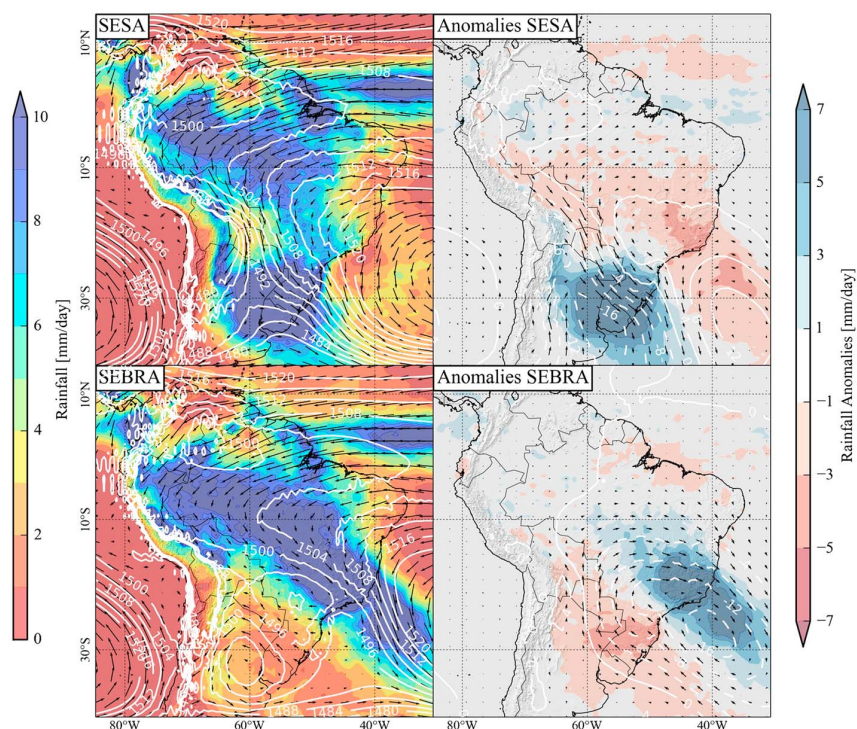
Figure 2. (left) Composites for the (top) SESA and (bottom) SEBRA phase: daily rainfall (background) and geopotential height (white lines) and wind fields at 850 mbar (black lines). (right) Anomalies of the same variables with respect to DJF climatology.

4.2. Complex Network Measures

For DG, we allow synchronizations of extreme events within a maximum delay of 3 days ($\tau_{max} = 3$), while for DR we only consider synchronizations at the very same day ($\tau_{max} = 0$). The choice of two different maximal temporal delays is justified by the different climatological interpretations we provide for the two network measures DG and DR. Note that computing DG for $\tau_{max} = 2$ or $\tau_{max} = 1$ does not substantially change the results (Figures S1 and S2 in the supporting information).

4.3. DG

For the SESA phase (Figure 3, top left), we observe high values of DG over the ITCZ, the entire Amazon Basin, along the eastern slopes of the Andes from northern Peru to northern Argentina, as well as over SESA. In contrast, we find low DG values over the SEBRA.

For the SEBRA phase (Figure 3, bottom left), we observe a substantially different spatial pattern of DG than for the SESA phase. High DG values in the vicinity of the ITCZ are located farther north than for the SESA phase. Over most parts of the Amazon Basin, values are even higher than for the SESA phase. Most notably, the highest values are located over the SACZ, extending from the central Amazon Basin to the subtropical Atlantic Ocean around 30°S and 30°W.

Note that the maximum delay $\tau_{max} = 3$ only serves as an upper bound for the dynamical delay τ (equation (1)), assuring the unique association of events in the computation of ES. Typically, extreme events synchronize on time scales shorter than 3 days, as is evident from comparing the results of Figure 3 with corresponding results for $\tau_{max} = 1$ and $\tau_{max} = 2$ (shown in the supporting information).

4.4. DR

For the reason explained in section 3.5, directionality is calculated for networks constructed from ES with $\tau_{max} = 0$. For the SESA phase, we observe N-S oriented streamlines over eastern Brazil, which turn anti-clockwise when moving farther west toward the Peruvian and Bolivian Andes, where they are approximately
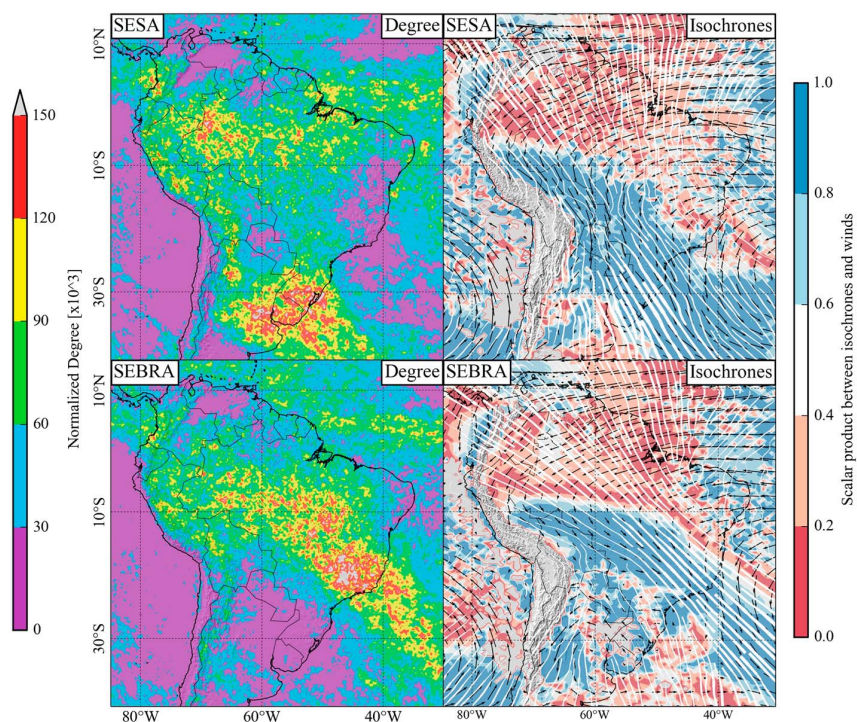
Figure 3. (left) Degree (DG) normalized by the respective link density of the network for the (top) SESA and (bottom) SEBRA phase. (right) Isochrones, wind fields at 850 mbar as well as the absolute value of the scalar product between wind vectors and isochrones for the SESA and the SEBRA phase.

NW-SE oriented. The most pronounced streamlines can be found over SESA, where they are also oriented in NW-SE direction. This orientation continues toward the SACZ, however, with reduced directionality strength DR^s (indicated by thinner streamlines).

For the SEBRA phase, the N-S oriented streamlines over northern Brazil rotate stronger than for the SESA phase when moving westward, with streamlines over central Brazil already oriented in NW-SE direction. We observe a clear pattern of almost straight, parallel streamlines extending from the central Amazon Basin southeastward across the southeastern Brazilian coast to the subtropical Atlantic Ocean. In contrast to the SESA phase, no streamlines can be observed over SESA.

For both dipole phases, we computed the scalar product between normalized wind vectors at 850 mbar (near surface) and normalized DR at each grid point in order to estimate the influence of the wind fields on the direction of extreme event propagation. We take the absolute value of the scalar product, since DR only yields an angle determining the orientation of network links rather than the actual direction. If the scalar product is close to 0, the orientation of extreme event propagation is approximately parallel to the wind direction, while for values close to 1, it will be approximately perpendicular.

For the SESA phase (Figure 3, top right), we observe small values (between 0 and 0.4) over almost the entire tropical part of South America between 10°N and 10°S, while the subtropics are characterized by values between 0.6 and 1.0. In particular, at the eastern slopes of the Central Andes in southern Peru and Bolivia as well as in SESA, the angles determined by DR are close to the wind angles.

For the SEBRA phase, the scalar product indicates that DR angles and wind vectors are perpendicular over the entire tropics between 10°N and 10°S. However, south of 10°, we find high values for the scalar product between wind vectors and DR angles extending from Bolivia east of the Andes to eastern Brazil. In particular over the climatological position of the SACZ, wind vectors and DR angles are typically parallel.

When subtracting the DG field for the SEBRA phase from the DG field obtained for the SESA phase (Figure 4), the dipole between the two phases becomes clearly recognizable: Highest positive values are
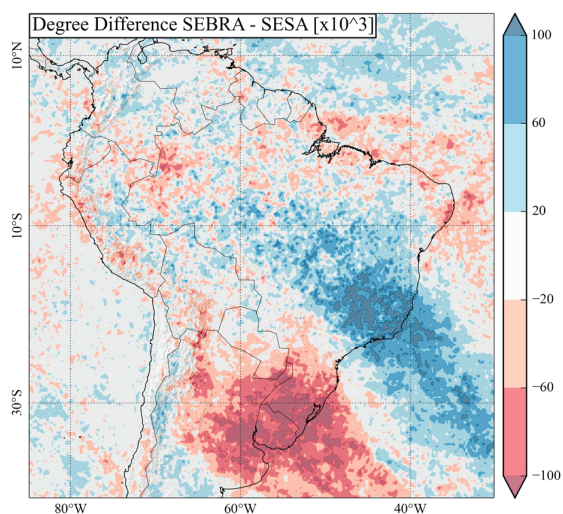
Figure 4. Difference between degree fields for the SEBRA and for the SESA phase. Note the oscillation between positive and negative values extending over the entire continent beyond the dipole between the SESA and SEBRA regions.

located over SESA, while highest negative values can be observed over SEBRA. However, it also becomes apparent that the oscillation is not confined to the dipole between SESA and SEBRA but farther extends over the remaining parts of the South American continent, although with smaller amplitude: Southwest of SESA, we observe negative values, while northeast of the SACZ, around the equator, we find positive values for the DG difference. North of 5°N, we observe negative values again.

5. Discussion

DG yields an estimate of the importance of a given grid point for the synchronization paths of extreme events over the continent, as expressed by the number of other grid points where extreme events occur synchronously with extreme events at this grid point. It should be emphasized, however, that this does not imply that single rainfall clusters propagate along the entire signature of high DG values, but rather that possibly different extreme events synchronize along this signature.

Complementarily, DR provides the typical orientation along which extreme events synchronize. According to our interpretation that rainfall events propagate in direction perpendicular to the DR streamlines, and further assuming that rainfall events in tropical South America propagate from east to west rather than from west to east [e.g., *Zhou et al.*, 1998; *Vera et al.*, 2006; *Marengo et al.*, 2012], we infer the following main climatological propagation pathways:

1. For the SESA phase, rainfall events originating from the tropical and subtropical Atlantic Ocean enter the continent at the northern Brazilian coast and propagate westward over the Amazon Basin (Figure 3, top row). Extreme events synchronize according to the direction dictated by the low-level wind fields until they reach the western part of the Amazon Basin. As soon as they turn southward toward the Peruvian and Bolivian Andes, the streamlines of simultaneous occurrence of extreme events are aligned with the wind direction. This can be explained by the orographic impact of the Andes mountains [*Bookhagen and Strecker*, 2008]: When the moist air is driven toward the mountains, it is lifted and causes extreme rainfall along the entire eastern slope of the Central Andes, extending from Peru to Bolivia. At the same time, the orography forces the low-level winds southward along the mountain slopes. South of 20°, we observe a pronounced propagation pattern over SESA, which implies synchronization of extreme rainfall events in a SW-NE direction. This is consistent with studies of extratropical cyclones and frontal systems, which move from southern Argentina northeastward, causing abundant rainfall over SESA [*Siqueira and Machado*, 2004; *Seluchi and Garreaud*, 2006]. In SESA, wind directions are perpendicular to the direction along which extreme rainfall events synchronize, which is typical for rainfall caused by these frontal systems, since the low-level winds from the north follow the isobars and interact with the frontal systems (Figure 2, top right). Thus, we infer that the synchronization direction of extreme events in the tropics is determined by the low-level flow, while in the subtropics and extratropics, the influence of frontal systems is dominant.

2. For the SEBRA phase, extreme events also propagate from the tropical Atlantic Ocean westward to the Amazon Basin but then occur simultaneously (i.e., at the same day) in a large area extending from the central Amazon Basin to the southeastern Brazilian coast and the adjacent subtropical Atlantic Ocean (Figure 4). The orientation of isochrones suggests that they synchronize in NE-SW orientation, i.e., perpendicular to the wind direction, implying that frontal systems approaching from the south play the most pronounced role for driving extreme rainfall in SEBRA.

The difference between the DG fields obtained for the SEBRA and SESA phases suggests an oscillation over the entire continent rather than a single dipole between the regions SESA and SEBRA. While these two regions are clearly the most pronounced, the alternating pattern extends from central Argentina beyond the equator, with three maxima and two minima in total between 40°S and 15°N. During austral summer, large-scale circulation patterns in the form of Rossby waves, which emanate from the western Pacific Ocean, induce northward propagating cold fronts in subtropical South America [*Hoskins and Ambrizzi*, 1993; *Rodwell and Hoskins*, 2001]. The observed oscillation suggests that these Rossby waves control extreme rainfall variability over the entire South American continent.

6. Conclusion

We studied the dynamical properties of extreme rainfall in the two most densely populated areas in South America: southeastern South America (SESA) including Buenos Aires and southeastern Brazil (SEBRA) around Saõ Paulo and Rio de Janeiro. A dipolar pattern of average rainfall between these two regions has previously been identified as the leading mode of intraseasonal variability in the South American monsoon system. In order to study the dynamical properties of extreme rainfall events associated with this dipole, we employed a combination of a nonlinear synchronization measure and complex network theory. This approach allowed us to identify the pathways of extreme rainfall synchronization and the network strength along these pathways. By constructing separate networks for the two phases of the rainfall dipole between SESA and SEBRA, we can distinguish the climatological synchronization routes of extreme rainfall for the two regimes: For the SESA phase, this route leads from the southern edge of the Intertropical Convergence Zone (ITCZ) across the Amazon Basin and subsequently southward along the Andes mountains to SESA. For the SEBRA phase, this path enters the continent north of the ITCZ and, after passing the Amazon Basin, turns southeastward to the SEBRA. By comparing climatological wind directions with the orientations of streamlines of synchronous extreme rainfall, we reveal a transition of driving mechanisms from the tropics to the subtropics: extreme rainfall propagation in the tropics is driven directly by the (mainly easterly) low-level winds, but extreme rainfall propagation in the subtropics is dominated by frontal systems approaching from the southern tip of the continent.

Our results indicate that the rainfall dipole between SESA and SEBRA is only the most prominent part of an oscillation which extends over the entire South American continent. This suggests that indirect influences of Rossby waves originating from the Pacific Ocean on extreme rainfall extend to tropical latitudes even beyond the equator.

References

Barros, V., R. Clarke, and P. Dias (2006), *Climate Change in the La Plata Basin*, Inter - Am. Inst. for Global Change Res., São José dos Campos, Brazil.

Berbery, E. H., and V. R. Barros (2002), The hydrologic cycle of the La Plata basin in South America, *J. Hydrometeorol.*, *3*(6), 630–645.

Boers, N., B. Bookhagen, N. Marwan, J. Kurths, and J. Marengo (2013), Complex networks identify spatial patterns of extreme rainfall events of the South American Monsoon System, *Geophys. Res. Lett.*, *40*, 4386–4392, doi:10.1002/grl.50681.

Boers, N., R. V. Donner, B. Bookhagen, and J. Kurths (2014), Complex network analysis helps to identify impacts of the El Niño Southern Oscillation on moisture divergence in South America, *Clim. Dyn.*, doi:10.1007/s00382-014-2265-7, in press.

Bookhagen, B., and M. R. Strecker (2008), Orographic barriers, high-resolution TRMM rainfall, and relief variations along the eastern Andes, *Geophys. Res. Lett.*, *35*, L06403, doi:10.1029/2007GL032011.

Carvalho, L. M. V., C. Jones, and B. Liebmann (2002), Extreme precipitation events in southeastern South America and large-scale convective patterns in the South Atlantic convergence zone, *J. Clim.*, *15*(17), 2377–2394.

Carvalho, L. M. V., C. Jones, and B. Liebmann (2004), The South Atlantic convergence zone: Intensity, form, persistence, and relationships with intraseasonal to interannual activity and extreme rainfall, *J. Clim.*, *17*(1), 88–108.

Durkee, J. D., T. L. Mote, and J. M. Shepherd (2009), The contribution of mesoscale convective complexes to rainfall across subtropical South America, *J. Clim.*, *22*(17), 4590–4605.

Hoskins, B., and T. Ambrizzi (1993), Rossby wave propagation on a realistic longitudinally varying flow, *J. Atmos. Sci.*, *50*(12), 1661–1671.

Huffman, G., D. Bolvin, E. Nelkin, D. Wolff, R. Adler, G. Gu, Y. Hong, K. Bowman, and E. Stocker (2007), The TRMM Multisatellite Precipitation Analysis (TMPA): Quasi-global, multiyear, combined-sensor precipitation estimates at fine scales, *J. Hydrometeorol.*, *8*(1), 38–55, doi:10.1175/JHM560.1.

Jorgetti, T., P. L. da Silva Dias, and E. D. de Freitas (2013), The relationship between South Atlantic SST and SACZ intensity and positioning, *Clim. Dyn.*, *42*(11-12), 3077–3086, doi:10.1007/s00382-013-1998-z.

Liebmann, B., G. N. Kiladis, C. S. Vera, A. C. Saulo, and L. M. V. Carvalho (2004), Subseasonal variations of rainfall in South America in the vicinity of the low-level jet east of the Andes and comparison to those in the South Atlantic convergence zone, *J. Clim.*, *17*(19), 3829–3842.

Malik, N., B. Bookhagen, N. Marwan, and J. Kurths (2012), Analysis of spatial and temporal extreme monsoonal rainfall over South Asia using complex networks, *Clim. Dyn.*, *39*(3), 971–987, doi:10.1007/s00382-011-1156-4.

Marengo, J., M. Valverde, and G. Obregon (2013), Observed and projected changes in rainfall extremes in the Metropolitan Area of São Paulo, *Clim. Res.*, *57*, 61–72, doi:10.3354/cr01160.

Marengo, J. A., W. R. Soares, C. Saulo, and M. Nicolini (2004), Climatology of the low-level jet east of the Andes as derived from the NCEP-NCAR reanalyses: Characteristics and temporal variability, *J. Clim.*, *17*(12), 2261–2280.

Marengo, J. A., et al. (2012), Recent developments on the South American monsoon system, *Int. J. Climatol.*, *32*(1), 1–21, doi:10.1002/joc.2254.

Monahan, A. H., J. C. Fyfe, M. H. P. Ambaum, D. B. Stephenson, and G. R. North (2009), Empirical orthogonal functions: The medium is the message, *J. Clim.*, *22*(24), 6501–6514, doi:10.1175/2009JCLI3062.1.

Nicolini, M., A. C. Saulo, J. C. Torres, and P. Salio (2002), Enhanced precipitation over southeastern South America related to strong low-level jet events during austral warm season, *Meteorologica, Special Issue for the South American Monsoon System*, *27*, 59–69.

Nogués-Paegle, J., and K. C. Mo (1997), Alternating wet and dry conditions over South America during summer, *Mon. Weather Rev.*, *125*(2), 279–291.

Quiroga, R. Q., T. Kreuz, and P. Grassberger (2002), Event synchronization: A simple and fast method to measure synchronicity and time delay patterns, *Phys. Rev. E*, *66*(4), 041904.

Rienecker, M. M., et al. (2011), MERRA: NASA's modern-era retrospective analysis for research and applications, *J. Clim.*, *24*, 3624–3648, doi:10.1175/JCLI-D-11-00015.1.

Rodwell, M., and B. Hoskins (2001), Subtropical anticyclones and summer monsoons, *J. Clim.*, *14*, 3192–3211.

Salio, P., M. Nicolini, and E. J. Zipser (2007), Mesoscale convective systems over southeastern South America and their relationship with the South American low-level jet, *Mon. Weather Rev.*, *135*(4), 1290–1309, doi:10.1175/MWR3305.1.

Seluchi, M., and R. Garreaud (2006), Influence of the subtropical Andes on baroclinic disturbances: A cold front case study, *Mon. Weather Rev.*, *134*(11), 3317–3335.

Siqueira, J., and L. T. Machado (2004), Influence of the frontal systems on the day-to-day convection variability over South America, *J. Clim.*, *17*, 1754–1766.

Vera, C., et al. (2006), Toward a unified view of the American monsoon systems, *J. Clim.*, *19*, 4977–5000.

Zhou, J., K. M. Lau, J. O. F. Climate, and G. Space (1998), Does a monsoon climate exist over South America?, *J. Clim.*, *11*(5), 1020–1040.